VNU Journal of Science:
Computer Science and Communication Engineering
Journal homepage: http://www.jcsce.vnu.edu.vn/index.php/jcsce

An Adaptive and Wide-Range Output DC-DC Converter for Loading Circuit of Li-Ion Battery Charger

Nguyen Van Hao, Nguyen Duc Minh, Pham Nguyen Thanh Loan*

BKIC Lab, School of Electronics and Telecommunications,
Hanoi University of Science and Technology, Hanoi, Vietnam

Abstract

In this paper, an adaptive and wide-range output DC-DC converter designed for lithium-ion (Li-Ion) battery charger circuit is proposed. The converter operates in continuous conduction mode (CCM) to provide an output voltage in response to battery voltage and a wide-range output current to ensure that circuit requirements are met. This circuit is designed on Cadence using 0.35-µm BCD technology. Simulation results show that the circuit fully operates in CCM mode with a load current from 50 mA to 1000 mA and output voltage ripple factor is less than 1 %. Furthermore, the current supplied to the load circuit responses to three types of Li-Ion rechargeable currents. The output voltage of the converter varies from 2.8 to 4.5 V corresponding to the voltage range of the battery being charged from 2.5 to 4.2 V. The average power efficiency of the converter in large load current mode (1000 mA) reaches 94 %.

Received 12 April 2018, Revised 18 June 2018, Accepted 18 June 2018

Keywords: Li-Ion battery, charging mode, charger circuit, DC-DC converter, adaptive reference voltage.

1. Introduction

Today, Li-Ion batteries are widely used in consumer electronics for its significant advantages such as high energy density, high recharge cycle (> 1000 cycles), no memory effect, low self-discharged rate (2 - 8 % per month), wide range of operating condition (charge at –20 – 60 °C, discharge at -40 - 65 °C). In addition, a single cell of Li-Ion battery can operate in the range of 2.5 to 4.2 V [1]. The charging circuit is designed according to three modes following the charging standard [2, 3] as shown in figure 1. Trickle constant current mode (TC) occurs when the battery voltage is less than 2.9 V, large constant current mode (LC) when the battery voltage is in the range of 2.9 to 4.2 V, and constant voltage charging mode (CV) when the battery voltage reaches 4.2 V.

In [4-6], the charging circuit is designed based on the structure of a low dropout regulator which offers high integration, fast and accurate control. But this charging structure has low power efficiency due to large deviation between supply voltage and battery voltage. To overcome this drawback, some techniques were proposed and presented in [7, 8].

* Corresponding author. loan.phamnguyenthanh@hust.edu.vn
https://doi.org/10.25073/2588-1086/vnucsce.194

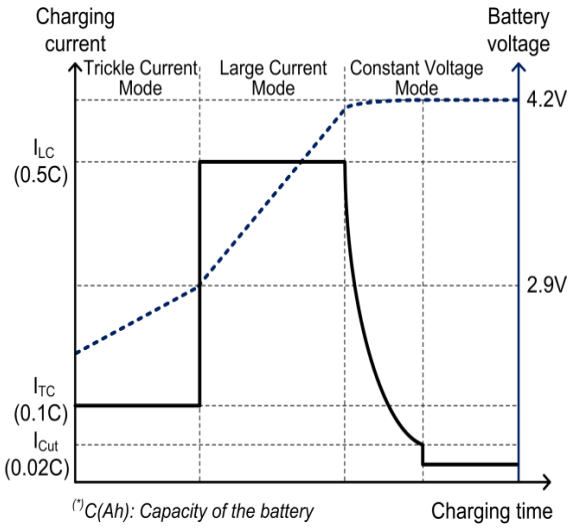

Figure 1. Li-Ion battery charging modes.

The switching mode power supply converter is used to generate a variable supply voltage changing in response to the battery voltage during the charging process. However, the use of large off-chip elements for the boost converter structure in [7] and the flyback converter in [8] increase the size of printed circuit board (PCB). The rechargeable circuit in [9, 10] adopted the buck converter structure minimizing the size of PCB. However, the TC charging mode was not introduced and there was no isolation between DC-DC converter and battery so the self-discharge of battery may occur and battery performance cannot be guaranteed. In this article, we propose an adaptive buck DC-DC converter based on a buck converter structure that operates in continuous conduction mode (CCM) with a wide range of voltage and current variations in accordance with the Li-Ion charging circuit that was presented in our previous work [11].

The rest of the paper is structured as follows: Section 2 describes the structure of an adaptive and wide-range output DC-DC converter with a battery charger as load. Design parameters are considered and calculated in Sub-Section 2 to ensure that the converter operates stably in CCM mode and can supply a wide range of voltage and current to the load circuit. In Section 3, the simulation results are shown to evaluate the converter's performance. Finally, the conclusion is given in Section 4.

2. Circuit descriptions

In general, the PWM DC-DC converter, as shown in figure 2, is implemented to provide a stable output voltage V_O from the input voltage V_I thanks to the closed loop control. The feedback voltage V_{FB} is sampled from the output through a voltage divider of two resistors R_{F1}, R_{F2}. In the compensator, the V_{FB} will be compared with the reference voltage V_{ARV} to generate the deviation voltage V_C which is used to determine the duty cycle of V_{PWM} from the PWM generator circuit. The switching signals V_N, V_P to the gate of two power MOSFET N and P are finally generated by the non-overlap gate driver. The output filter LC_O is well chosen to stabilize the output voltage that can be determined as follows (1)

$$V_O = \left(\frac{R_{F1} + R_{F2}}{R_{F2}}\right) V_{ARV} \quad (1)$$

Besides, the load of this DC-DC converter is a Li-Ion battery charging circuit which has been implemented in [11]. In that previous work, the varying battery voltage V_{Bat} during the charging process is fed into the voltage level-shift circuit to provide a variable reference voltage V_{ARV}, which is also called an adaptive reference voltage. The DC-DC converter's output voltage V_O should also be controlled to follow the battery voltage V_{Bat} so that the power efficiency of the whole system is improved. In this design, the value of the input voltage V_I is. around 6 V, switching frequency F_{SW} is selected at 500 KHz and the output voltage V_O of the converter is expected to be always 0.3 V higher than the battery voltage V_{Bat}.

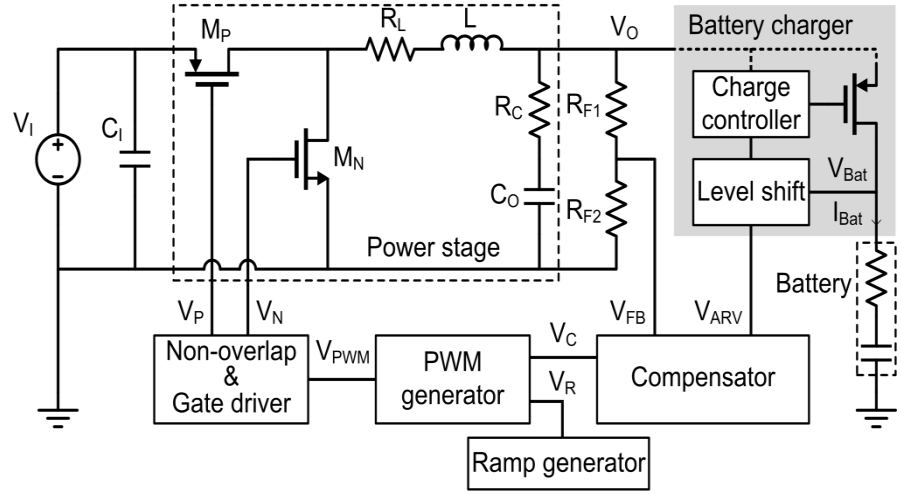

Figure 2. Structure of adaptive DC-DC converter with Li-Ion battery charger as load.

2.1. Compensator

To ensure the current and voltage requirements to the load circuit, the analysis of a conventional buck converter presented in [12] is employed to determine the value of inductor L and the ceramic capacitor C_O. The theoretical calculation pointed out that the corresponding values of inductor and capacitor should be 22 µH ($R_L \approx 46$ mΩ) and 22 µF ($R_C \approx 5$ mΩ) respectively. The transfer function of power converter stage is thus defined as a function of double-pole ω_{LC} (7.23 KHz) generated by the LC_O filter and one zero ω_{ESR} (1.45 MHz) created by the equivalent series resistance R_C and C_O. To stabilize the circuit and compensate the phase degradation caused by the double-pole, the type-III compensation is adopted as shown in figure 3. Error amplifier EA is designed using a class AB two-stage op-amps with high and symmetrical slew rate [13]. Transfer function of the compensation circuit given in (2) consists of three poles (ω_{P0}, ω_{P1}, ω_{P2}) and two zeros (ω_{Z1}, ω_{Z2}). The zero frequency ω_{ESR} is much larger than the switching frequency ω_{SW} so that it does not affect the frequency range of the converter. In this approach, zero frequencies ω_{Z1} and ω_{Z2} are designed in adjacent to the double-pole at frequencies $0.6\omega_{LC}$ and $1.5\omega_{LC}$ respectively. Pole frequency ω_{P1} is set at $0.5\omega_{SW}$ and ω_{P2} is calibrated in frequency range of $(0.8 – 0.9)\omega_{SW}$.

$$K_C(s) = \frac{1}{R_{F1}(C_2 + C_3)} \frac{1}{s} \frac{\left(1+\frac{s}{\omega_{Z1}}\right)\left(1+\frac{s}{\omega_{Z2}}\right)}{\left(1+\frac{s}{\omega_{P1}}\right)\left(1+\frac{s}{\omega_{P2}}\right)} \quad (2)$$

With,

$$\omega_{P0} = 0, \quad \omega_{P1} = \frac{1}{R_1 C_1}, \quad \omega_{P2} = \frac{1}{R_2\left(\frac{C_2 C_3}{C_2 + C_3}\right)}$$

$$\omega_{Z1} = \frac{1}{R_2 C_2}, \quad \omega_{Z2} = \frac{1}{C_1(R_1 + R_{F1})}$$

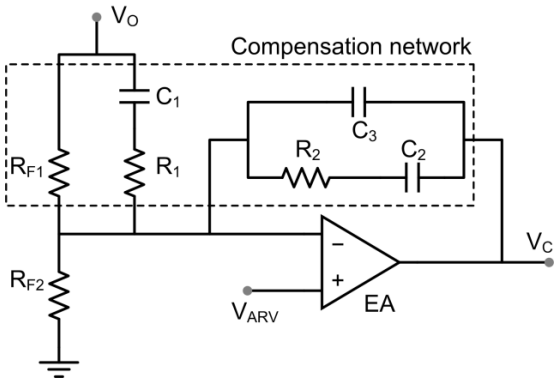

Figure 3. Type-III compensation circuit.

Table 1. List of components

Resistors	Parameters	Capacitors	Parameters
R_{F1}, R_{F2}	13 KΩ	C_1	1100 pF
R_1	566 Ω	C_2	510 pF
R_2	71.5 KΩ	C_3	5.1 pF

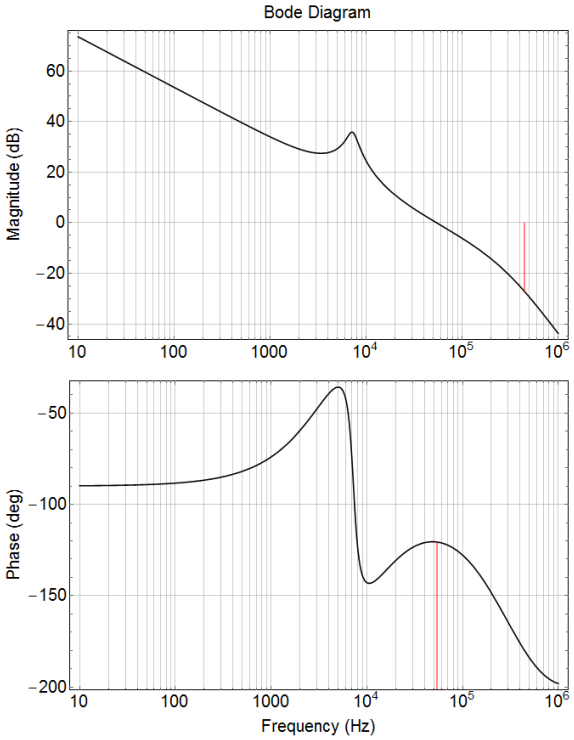

Figure 4. Bode plot of the converter's loop gain for $V_0 = 4$ V and $I_0 = 1$ A.

From (2), the design values of the compensation network components are calculated and summarized in table 1. The phase margin and gain margin in figure 4 demonstrated a loop gain of converter ~ 59.4 deg at cross frequency 54 KHz and 27 dB at frequency 445 KHz.

2.2. PWM generator

In figure 5(a), the high-speed comparator is used [14] to provide pulse width modulator (PWM) signals. As mentioned above, the signal V_C is compared to ramp signal V_R at fixed amplitude and frequency to produce the pulse signal V_{PWM} where its duty cycle D is defined as in (3). The waveforms of V_C, V_R and V_{PWM} are illustrated in figure 5(b). The PWM circuit functions correctly as expected through the loop control and it is able to regulate the output voltage of DC-DC converter.

$$\frac{V_O}{V_I} = D = \frac{V_C}{V_R} \quad (3)$$

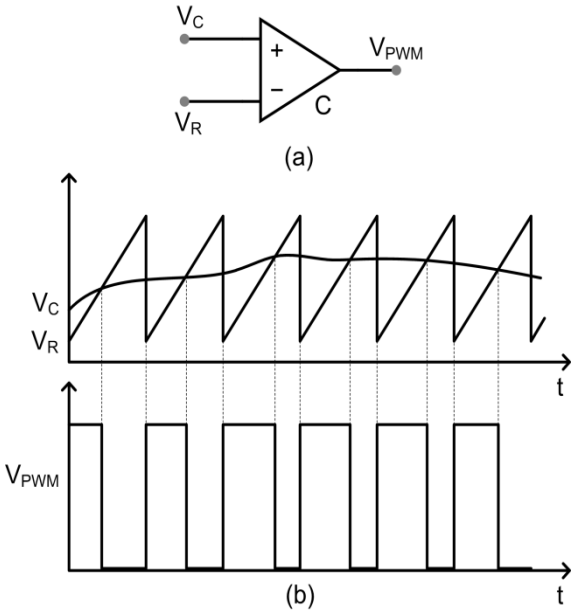

Figure 5. (a) PWM generation circuit. (b) Corresponding signals.

2.3. Ramp generator

The schematic of a ramp generator is shown in figure 6(a). The reference current I_B is created and controlled by reference voltage V_{Ref} as a current source. The topology of low-voltage cascode current mirror is used to create the currents I_R and I_{Ch}. The reference voltages V_H and V_L are then created by the flow of current I_R through two resistors R_H and R_L in series. The ramp signal is produced by the charging and discharging of the capacitor C_R. In steady state, when $V_L < V_R < V_H$, the transistors $M_{10} - M_{12}$ are OFF, the reference voltage V_H is connected to the negative input of the

comparator. The capacitor C_R is then charged during this period until the voltage V_R is higher than V_H. That will turn the transistors $M_{10} - M_{12}$ ON so the reference voltage is switched to V_L. The capacitor C_R is discharged rapidly, the voltage V_R is reduced to a value smaller than V_L that turn the transistors $M_{10} - M_{12}$ to OFF state. The process is then repeated. The period of ramp signal is calculated as a function of the charging time (T_{rise}) as expressed in equation (4) and the discharging time (T_{fall}) of the capacitor C_R. The ratio of T_{fall}/T_{rise} is approximately of 5 % that lead to a discharging time T_{fall} of about 100 ns.

$$T_{rise} = \frac{(V_H - V_L)C_R}{I_{Ch}} = \frac{I_R R_H C_R}{I_{Ch}} = R_H C_R \qquad (4)$$

As can be seen in equation (4), the value of ramp frequency is a function of R_H and C_R. To ensure the performance of ramp generator, a high gain OA [15] with loop gain stability is adopted. The high speed comparator C is designed with a propagation delay of about 10 ns that is suitable for our adaptive-output converter. Simulations of ramp generator is presented in figure 6(b). It can be seen that ramp signal V_R meets the maximum value at 3.51 V and minimum value at 0.45 V where the operating signal reaches 500.5 KHz as expected.

2.4. Non-overlap and Gate Driver

The non-overlap and gate driver circuit are illustrated in figure 7(a). The gate driver is a buffer circuit consisting of four inverter layers designed according to the tapering factor in the range of 3 to 4 [14]. The gate driver is used to switch the power transistors M_P and M_N of DC-DC converter to obtain a certain output voltage level defined by the duty cycle of switching control signal V_{PWM}. In addition, to avoid power loss induced at each switching transition when both M_P and M_N are open resulting in shoot-through current loss, the non-overlap circuit is also implemented. A sufficient small delay between the rise time and fall time of two opposite V_P and V_N signals is added. Their waveforms are presented in figure 7(b).

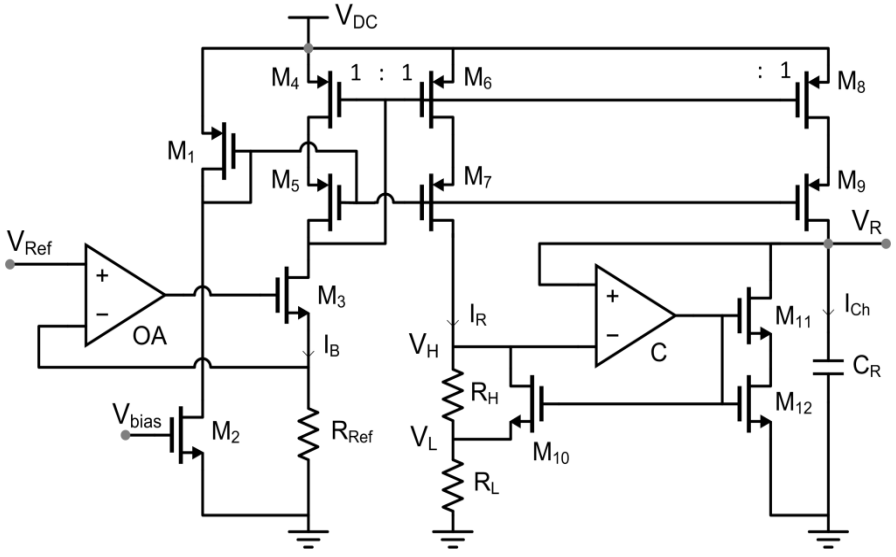

(a)

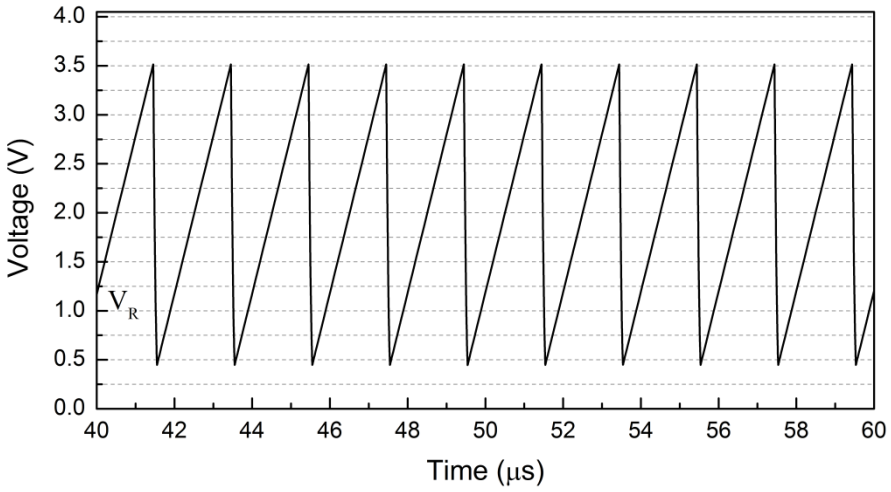

(b)

Figure 6. (a) Ramp generation circuit. (b) Waveform of ramp signal.

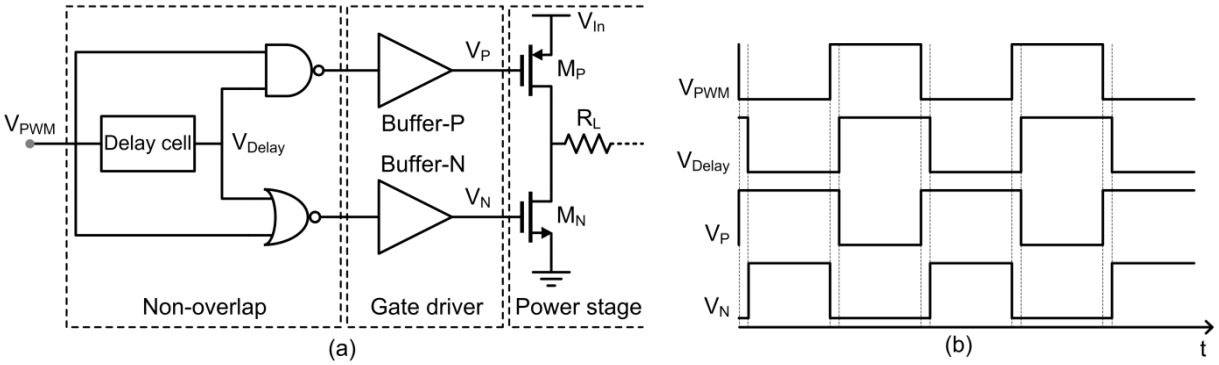

Figure 7. (a) Non-overlap and gate driver. (b) Corresponding output waveforms.

3. Simulation results

The inductor current and output voltage of the proposed DC-DC converter are shown in figure 8. It is obvious that the continuous conduction mode is guaranteed for three different operation modes of battery charging circuit playing the role as load of the converter. The average inductor current, also called as the load current, reaches the value of 200 mA at output voltage of 3 V, 1000 mA with output voltage of 4 V and 50 mA with output voltage of 4.5 V, respectively. These results confirm that the circuit meets the requirement of power supply for battery charging circuit while it works at trickle charging mode (TC), large current charging mode (LC) and constant voltage charging mode (CV) respectively. Besides, the output voltage ripple is relatively small and almost lower than 1 %.

In figure 9(a), it can be observed that the results show smooth and stable transitions of load current from trickle mode (200 mA) to large current mode (1000 mA) and then to constant voltage mode (50 mA). This current profile meets completely the charging profile of a Li-Ion battery charger. It means that the proposed compensation circuit and the control loop including PWM and gate driver work effectively and guarantee the stability of the

whole system. At light load, when the load current is less than 50 mA, the converter gradually switches to DCM mode, that results in power loss. But this problem can be improved by a detecting-negative-current circuit from the inductor current of the power stage. In addition, a slight undershoot voltage at the transition from trickle to large current mode is also observed in figure 9(b). However, an undershoot voltage of 60 mV which is about 1.8 % of output voltage can be neglected. Interestingly, a constant 0.3 V difference between the output voltage V_O of the proposed DC-DC converter and the battery is recorded for three different charging modes. The converter's output voltage is always 0.3 V higher than the battery voltage. It is seen that V_O is adjusted dynamically according to the battery voltage with the accuracy of over 99 %. As per its name, this DC-DC converter provides an adaptive power supply, not a constant output voltage like any other conventional DC-DC converter, to the battery charger circuit.

As can be observed in figure 10, the power efficiency of our proposed adaptive-output converter is higher than 94 % for an output voltage varying widely from 2.8V to 4.5 V. The highest efficiency can be reached at 97 % where output voltage varies from 2.8 to 3.2 V and load current is 200 mA. Efficiency is 94 % with an output voltage varying from 3.2 V to 4.5 V where load current is 1000 mA.

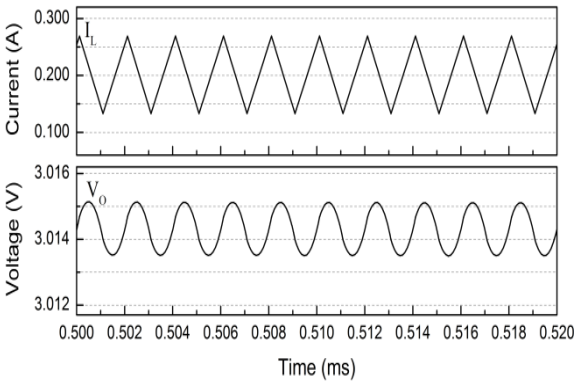

(a) Corresponding to TC mode of the battery charger

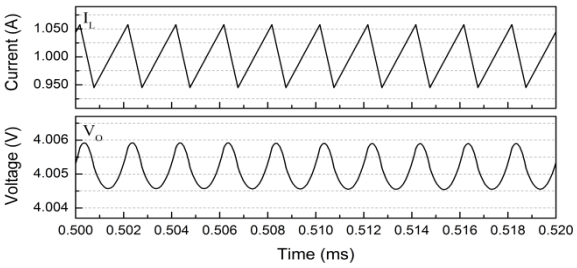

(b) Corresponding to LC mode of the battery charger

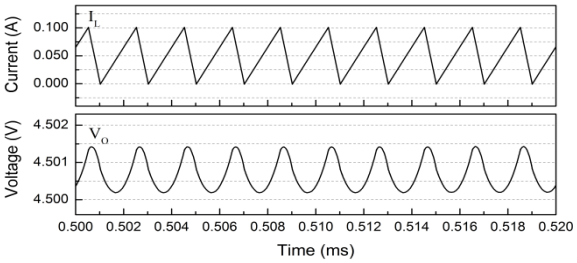

(c) Corresponding to CV mode of the battery charger

Figure 8. Steady-state waveforms of inductor current and output voltage with.

(a) I_O = 0.2 A, V_O = 3.0 V. (b) I_O = 1 A, V_O = 4.0 V. (c) I_O = 50 mA, V_O = 4.5 V.

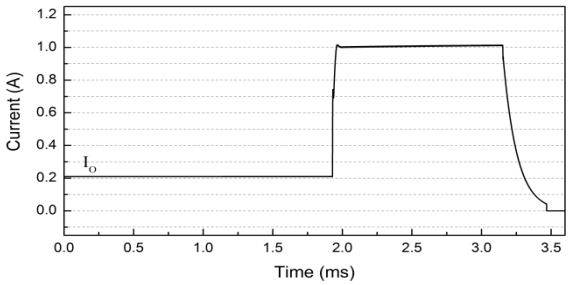

(a)

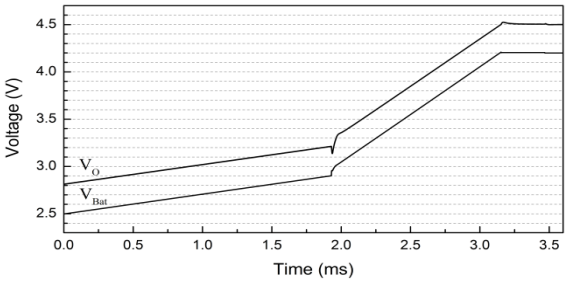

(b)

Figure 9. Simulation results of adaptive DC-DC converter with Li-Ion battery charger load.
(a) Output current.
(b) Output voltage and battery voltage.

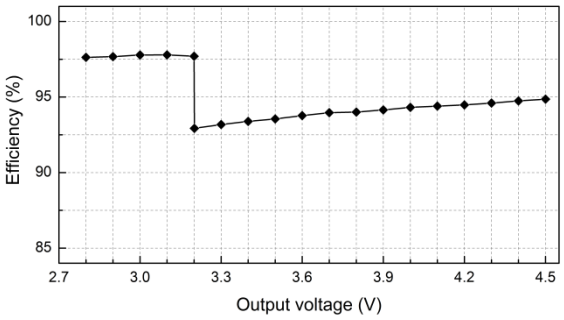

Figure 10. Power efficiency of adaptive DC-DC converter with versus output voltage.

4. Conclusion

An adaptive and wide-range output DC-DC converter for the Li-Ion battery charger circuit is proposed and designed on the 0.35 μm BCD technology. The converter operating in CCM mode offers a wide range of load current from 50 mA to 1000 mA as well as a broad range of voltage output (from 2.8 to 4.5 V) to the load circuit. The output current and voltage profile of the proposed converter meets perfectly the requirements for Li-Ion battery charger circuit. An average power efficiency of 94 % obtained for the crucial stage of large-current charging mode (1000 mA). As a continuation to our previous work, this circuit helps to complete a charging system from power line DC to a Li-Ion battery by combining with the battery charger in [11].

Acknowledgements

This research was supported by Prof. Lee Sang-Guk, NICE lab, KAIST, Korea.

References

[1] D. Linden, and T. B. Reddy, Handbook of batteries, ch. 35, pp. 35.2, New York: McGraw-Hill, 2002.

[2] S. Dearborn, "Charging Li-Ion batteries for maximum run times," Power Electron. Technol. Mag., pp. 40-49, Apr. 2005.

[3] A. A. Hussein and I. Batarseh, "A review of charging algorithms for nickel and lithium battery chargers," IEEE Trans. Veh. Tech., vol. 60, no. 3, pp. 830-838, Mar. 2011.

[4] C.-C. Tsai, C.-Y. Lin, Y.-S. Hwang, W.-T. Lee, T.-Y. Lee, "A multi-mode LDO-Based Li-Ion battery charger in 0.35-mm CMOS technology," IEEE Asia-Pacific Conf. Circuits Syst., 2004, pp. 49-52.

[5] C. C. Tsai, C. Y. Lin, Y. S. Hwang and T. Y. Lee, "The design of a Li-Ion battery charger based on multimode LDO Technology," Journal of Circuits, Systems and Computers, vol. 18, no. 05, pp. 947-963, 2009.

[6] Hieu M. Nguyen, Lam D. Pham and Trang Hoang, "A novel Li-Ion battery charger using multi-mode LDO configuration based on 350 nm HV-CMOS," Analog Integrated Circuits and Signal Processing, vol. 88, issue 3, pp. 505-516, Jun. 2016.

[7] M. Chen and G. A. Rincón-Mora, "Accurate, compact, and power-efficient Li-Ion battery charger circuit," IEEE Trans. Circuits Syst. II, Exp. Briefs, vol. 53, no. 11, pp. 1180-1184, Nov. 2006.

[8] J. Chen, F. Yang, C. Lai, Y. Hwang and R. Lee, "A high-efficiency multimode Li-Ion battery charger with variable current source and controlling previous state supply voltage," IEEE Trans. Ind. Electron., vol. 56, no. 7, pp. 2469-2478, Jul. 2009.

[9] R. Pagano, M. Baker and R.E. Radke, "A 0.18-μm monolithic Li-Ion battery charger for wireless devices based on partial current sensing and adaptive reference voltage," IEEE J. Solid-State Circuit, vol. 47, no. 6, pp. 1355-1368, Jun. 2012.

[10] T. C. Huang, R. H. Peng, T. W. Tsai, K. H. Chen and C. L. Wey, "Fast charging and high efficiency switching-based charger with continuous built-in resistance detection and automatic energy deliver control for portable electronics," IEEE Journal of Solid-State Circuits, vol. 49, no. 7, pp. 1580-1594, Jul. 2014.

[11] H. Nguyen-Van, T. Nguyen, V. Quan, M. Nguyen and L. Pham-Nguyen, "A topology of charging mode control circuit suitable for long-life Li-Ion battery charger," IEEE Sixth International Conference on Communications and Electronics, 2016, pp. 167-171.

[12] Byungcho Choi, Pulsewidth modulated DC-to-DC power conversion: circuits, dynamics, and control designs, John Wiley & Sons, 2013.

[13] J. Aguado-Ruiz, A. Lopez-Martin, J. Lopez-Lemus and J. Ramirez-Angulo, "Power Efficient Class AB Op-Amps With High and Symmetrical Slew Rate," IEEE Transactions on Very Large Scale Integration (VLSI) Systems, vol. 22, no. 4, pp. 943-947, Apr. 2014.

[14] Cheung Fai Lee and P. K. T. Mok, "A monolithic current-mode CMOS DC-DC converter with on-chip current-sensing technique," IEEE Journal of Solid-State Circuits, vol. 39, no. 1, pp. 3-14, Jan. 2004.

[15] J. Mahattanakul and J. Chutichatuporn, "Design Procedure for Two-Stage CMOS Opamp With Flexible Noise-Power Balancing Scheme," IEEE Transactions on Circuits and Systems I: Regular Papers, vol. 52, no. 8, pp. 1508-1514, Aug. 2005.